ACS Partner Journal

CHEMICAL & BIOMEDICAL IMAGING

Open Access

pubs.acs.org/ChemBioImaging

Article

A Near-Infrared Fluorescent Probe for Visualization of Acetylcholinesterase Flux in the Acute Epileptic Mice Brain

Li Fan,* Rui Wang, Qi Zan, Kunyi Zhao, Yuewei Zhang, Yunong Huang, Xue Yu,* Yongming Yang, Wenjing Lu, Shaomin Shuang, Xihua Yang,* and Chuan Dong*

Cite This: *Chem. Biomed. Imaging* 2025, 3, 332−340

Read Online

ACCESS | Metrics & More | Article Recommendations | Supporting Information

ABSTRACT: Neurotransmitter imbalance is an important pathological basis for epilepsy seizures. Acetylcholinesterase (AChE) as a key hydrolase in the cholinergic system directly affects the metabolism of neurotransmitter. Unfortunately, owing to the lack of reliable in situ imaging tools in the brain, the association between AChE and epilepsy has not been fully elucidated yet. Here, we rationally designed a near-infrared (NIR) fluorescent probe (**QXMC**) by employing *N*,*N*-dimethyl carbamyl as an AChE sensing group in the quinolinium-xanthene NIR skeleton. **QXMC** exhibited high sensitivity, excellent selectivity, and ultrafast response time (within 0.5 s) toward AChE. Moreover, **QXMC** can sensitively monitor the fluctuations of AChE activity in the neuronal cells and zebrafish during the apoptosis or oxidative stress process. Significantly, using **QXMC** with superb blood−brain barrier (BBB) permeability, for the first time, we discovered a down-regulated AChE level in the acute epileptic mice brain through noninvasive NIR in vivo imaging. Moreover, the visualization of therapeutic evaluation of epilepsy has also been achieved by monitoring AChE with **QXMC**. This work demonstrated the great potential of **QXMC** as an effective imaging tool for epilepsy diagnosis, therapeutic evaluation, and pathogenesis study.

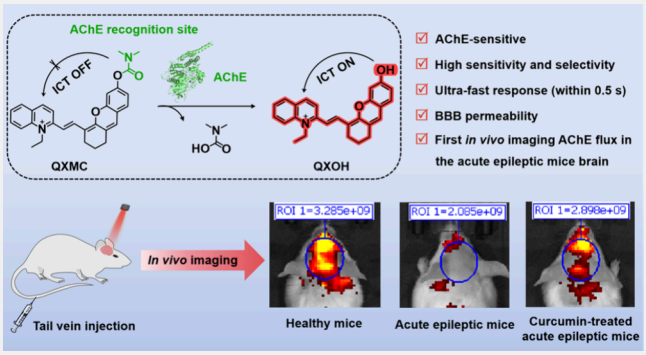

KEYWORDS: *Fluorescent probe, Near-infrared (NIR), Acetylcholinesterase (AChE), Epilepsy, Fluorescence imaging*

INTRODUCTION

Epilepsy is one of the most common chronic central nervous system diseases that affects over 50 million people worldwide.[1] Epilepsy is a syndrome characterized by episodic, transient, repetitive, and typically stereotyped central nervous system dysfunction caused by highly synchronized and excessive discharge of brain neurons due to different etiologies.[2] Although the seizures of most epilepsy patients can be controlled through antiepileptic drug treatment, about 30% of patients are resistant to drugs and become refractory epilepsy,[3] making the diagnosis and therapy of epilepsy still a major challenge in neuroscience and clinical medicine.

Previous studies indicated that epileptic seizures involved an imbalance between excitability and inhibition in the central nervous system.[2] Neurotransmitter is the main excitatory and inhibitory structure of the central nervous system, in which the excess of excitatory neurotransmitter or the deficiency of inhibitory neurotransmitter can lead to neuronal activity disorder, suggesting that the neurotransmitter imbalance (or dysfunction) is closely related to epileptic seizures. Acetylcholine (ACh) is an important neurotransmitter in the central cholinergic system, which can be released into the synaptic cleft to transmit neural signal when nerve endings are stimulated by excitation.[4] Acetylcholinesterase (AChE) as a key hydrolase in the cholinergic system can cleave ACh and render it inactive, thereby maintaining the balance of ACh.[5] Obviously, abnormal fluctuations in AChE activity directly affect the metabolism of ACh and disrupt neural signal transmission in the brain. This will inevitably affect emotions and behavior, ultimately resulting in neurological disorders such as Alzheimer's disease,[6] depression,[7] and epilepsy,[8] etc. However, due to the complexity of the brain and the lack of suitable tools, the changes in AChE activity and the associated molecular mechanisms involved in epileptic seizures remain uncertain. For example, previous research showed that ACh accumulated abnormally in the brain during the early stages of acute epileptic seizures, possibly owing to the decreased AChE activity.[8−10] But some studies have also found that AChE was upregulated in temporal lobe structures of status epilepticus-experienced epileptic rats.[11,12] Therefore, there is an urgent need to develop accurate and reliable methods for real-time in

Received: August 5, 2024
Revised: October 4, 2024
Accepted: October 7, 2024
Published: October 17, 2024

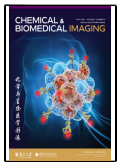

Scheme 1. Recognition Mechanism of QXMC toward AChE and Schematic Illustration of QXMC for In Vivo Imaging of AChE Flux in Epileptic Mice Brain

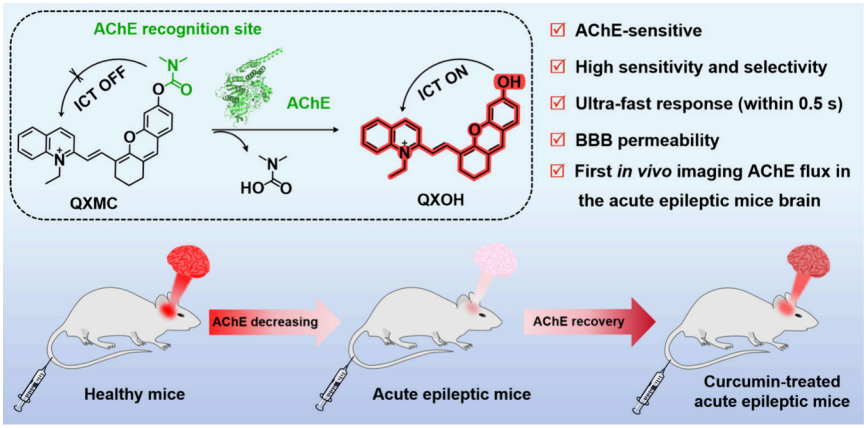

situ monitoring of AChE in the brain, which would help to better understand the pathological mechanisms of epilepsy as well as screen and evaluate the efficacy of antiepileptic drugs.

Fluorescent imaging based on fluorescent probes has recently captivated great attention for the dynamic monitoring of bioactive molecules at the level of cells, tissues, and even living animals, by virtue of its high sensitivity, excellent spatiotemporal resolution, noninvasive and visualized observation, real-time in situ response, simple operation, and fast feedback.[13−17] Although many fluorescent probes have been developed for AChE imaging in cells or tissues,[18−33] in vivo imaging tools for AChE detection in living brains are still lacking. It is known that the central nervous system has a natural blood−brain barrier (BBB), which can ensure brain energy supply and microenvironmental stability, but also restricts the passage of about 98% of small molecules and nearly all large molecules.[34] It is obvious that excellent BBB penetration ability is the prerequisite for fluorescent probes for achieving in vivo brain imaging. In 2019, Li and Tang et al. designed a merocyanine-based two-photo (TP) fluorescent probe (MCYN), displaying "turn-on" emission at 560 nm in the presence of AChE.[19] This is the only reported probe that can cross the BBB and has been applied for visualizing AChE in stress-induced depression phenotypes through TP fluorescence imaging. In general, near-infrared (NIR, around 650−1700 nm) fluorescence imaging is more suitable for the visualization of intact live animals, owing to its deep tissue penetration, lower spontaneous fluorescence and light scattering, and minimal tissue absorption.[35−37] Recently, a few NIR probes for imaging AChE activity in biosystems have been reported.[21−30] Nevertheless, to our knowledge, AChE-sensitive NIR probes with BBB penetrability have not been reported yet, especially the lack of research on real-time in situ visualization of AChE flux in epileptic mice brain.[38]

To address this issue, we engineered a novel fluorescent probe (((*E*)-2-(2-(6-((dimethylcarbamoyl)oxy)-2,3-dihydro-1*H*-xanthen-4-yl)vinyl)-1-ethylquinolin-1-ium, **QXMC**) for visualization of AChE activity in an epilepsy mice model by NIR fluorescence imaging (Scheme 1). **QXMC** contains a quinolinium-xanthene conjugated skeleton as the NIR fluorophore, and a *N*,*N*-dimethyl carbamyl as the AChE-sensitive group, which displays a remarkably enhanced NIR fluorescence response toward AChE with high sensitivity, excellent selectivity, as well as ultrafast response time. Significantly, **QXMC** has a superior BBB crossing ability, making it enormously suitable for the in vivo monitoring of AChE fluctuations in the brains. Facilitated by **QXMC**, noninvasive in vivo imaging of AChE flux in the brains of epilepsy model mice has been successfully achieved for the first time, making it a potential imaging tool for the diagnosis and treatment of AChE-related brain diseases.

EXPERIMENTAL SECTION

Materials and Instruments

The materials and apparatus used in this work are listed in the Supporting Information.

Synthesis

Details regarding the synthesis routine (Scheme S1), compounds **1**−**3**, QXOH ((*E*)-1-ethyl-2-(2-(6-hydroxy-2,3-dihydro-1*H*-xanthen-4-yl)vinyl)quinolin-1-ium), and characterizations of all compounds (Figures S1−S10) can be found in the Supporting Information.

Synthesis of QXMC

Compound QXOH (50 mg, 0.1 mmol) was dissolved in DMF (1 mL), and then K_2CO_3 (21 mg, 0.15 mmol) was added, with stirring for 30 min at room temperature. Dimethylcarbamoyl chloride (40 μL, 0.3 mmol) then was added, with stirring for 1 h at 50 °C. After completion of the reaction, distilled water (10 mL) was added, the organic phase was extracted with CH_2Cl_2/MeOH (10:1, v/v, 3 × 50 mL), then dried with anhydrous $MgSO_4$, evaporated, and purified by column chromatography to obtain **QXMC** as a purple solid (35 mg, 60% yield). ^{1}H NMR (400 MHz, DMSO-d_6) δ (ppm): 8.76 (d, J = 9.0 Hz, 1H), 8.64−8.58 (m, 2H), 8.42 (d, J = 9.0 Hz, 1H), 8.29 (d, J = 7.6 Hz, 1H), 8.09 (t, J = 7.8 Hz, 1H), 7.84 (t, J = 7.4 Hz, 1H), 7.40 (d, J = 8.4 Hz, 1H), 7.35 (d, J = 1.7 Hz, 1H), 7.08 (s, 1H), 6.98 (dd, J = 8.3, 2.0 Hz, 1H), 6.84 (d, J = 15.0 Hz, 1H), 4.98 (d, J = 7.0 Hz, 2H), 3.07 (s, 3H), 2.95 (s, 3H), 2.68 (s, 5H), 1.83 (s, 3H), 1.54 (t, J = 6.9 Hz, 4H). ^{13}C NMR (100 MHz, DMSO-d_6) δ (ppm): 155.20, 155.04, 153.97, 152.95, 152.87, 142.40, 141.93, 134.93, 130.61, 129.61, 128.48, 127.76, 127.27, 121.03, 119.20, 118.78, 118.39, 113.09, 112.70, 110.10. HR−MS m/z: $[M]^+$ calculated for $C_{29}H_{29}N_2O_3^+$, 453.2173; measured, 453.2168.

Visualization of AChE in Living Neuronal Cells, Zebrafish, and Epilepsy Model Mice

The cells and zebrafish imaging experiments and construction and imaging of epilepsy model mice were shown in the Supporting Information.

https://doi.org/10.1021/cbmi.4c00058
Chem. Biomed. Imaging 2025, 3, 332−340

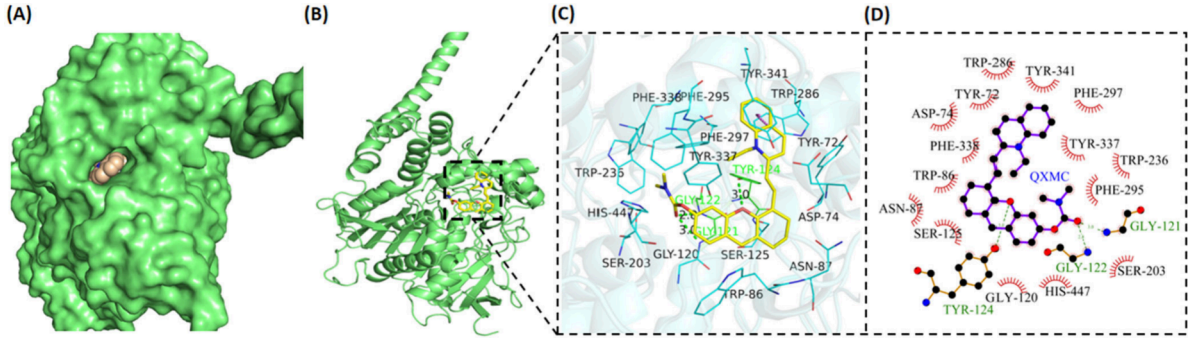

Figure 1. Binding mode of **QXMC** with AChE predicted by AutodockVina. (A,B) 3D structure of the **QXMC**−AChE complex. AChE is rendered in a green tube; **QXMC** is rendered in yellow. Detailed 3D (C) and 2D (D) binding modes between **QXMC** and AChE. Hydrogen bonding is rendered as a green dashed line; $\pi-\pi$ stacking interaction is rendered as a purple dashed line; and hydrophobic interaction is rendered as a red gear shape.

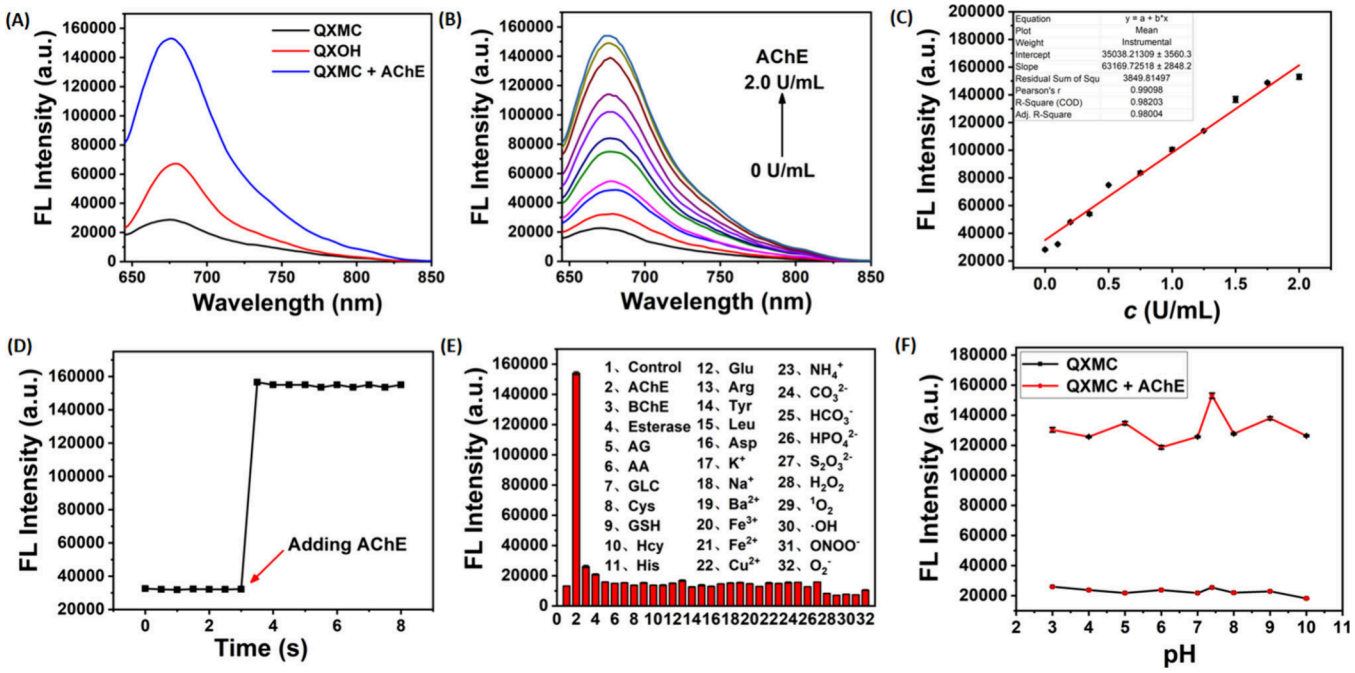

Figure 2. Optical response of **QXMC** toward AChE. (A) FL spectra of QXOH (5 μM) and **QXMC** (5 μM) with or without AChE (2.0 U/mL) in CH_3CN/PBS (1/49, v/v, pH 7.4, 10 mM). (B) FL spectra of **QXMC** (5 μM) in response to AChE (0−2.0 U/mL). (C) Linear relationship between $I_{678\,nm}$ and AChE activity (0−2.0 U/mL). (D) Time-course of **QXMC** (5 μM) in response to AChE (2.0 U/mL). (E) FL intensity of **QXMC** (5 μM) in the presence of various active species. (F) FL intensity of **QXMC** (5 μM) with or without AChE (2.0 U/mL) in the pH range of 3.0−10.0. λ_{ex} = 633 nm, λ_{em} = 678 nm.

RESULTS AND DISCUSSION

Design and Synthesis of AChE-Responsive QXMC

The fluorescent probe **QXMC** was designed by linking *N*,*N*-dimethyl carbamyl on the hydroxyl group of quinolinium-xanthene dye (QXOH). QXOH has long absorption and NIR emission that are beneficial for improving the quality of in vivo images. Moreover, inspired by carbamate in the structure of neostigmine (an effective AChE inhibitor), *N*,*N*-dimethyl carbamyl is selected as the AChE response group, which is expected to specifically bind to the "esteratic" subsite of AchE and cause it deactivation. Meanwhile, *N*,*N*-dimethyl carbamyl also served as a quenched moiety of the molecule that can inhibit the intramolecular charge transfer (ICT) process, making **QXMC** itself have very weak fluorescence. When *N*,*N*-dimethyl carbamyl is selectively recognized by the hydrolytic center of AChE, the ester bond is cleaved, and then QXOH is released, leading to a strong NIR fluorescent signal. More importantly, the quinoline quaternary ammonium (N^+) unit tends to interact with an "anionic" subsite of the hydrolytic center of AChE, which can enhance the affinity between **QXMC** and AChE, thereby improving hydrolysis efficiency.[19] Thus, the coupling of *N*,*N*-dimethylaminoformyl and quaternary ammonium groups is the important basis for designing AChE-specific probes through the "acetylcholine-mimic" approach.

We further conducted molecular docking simulations (using AutodockVina 4.2.6) to predict the binding interactions between **QXMC** and AChE molecules. As shown in Table S1, **QXMC** can spontaneously bind with the protein AChE with a binding energy of −8.903 kcal/mol, suggesting a high docking affinity between **QXMC** and AChE. Figure 1 depicted the rational docking mode and detailed binding interactions between **QXMC** and AChE, and it can be seen that **QXMC**

https://doi.org/10.1021/cbmi.4c00058
Chem. Biomed. Imaging 2025, 3, 332−340

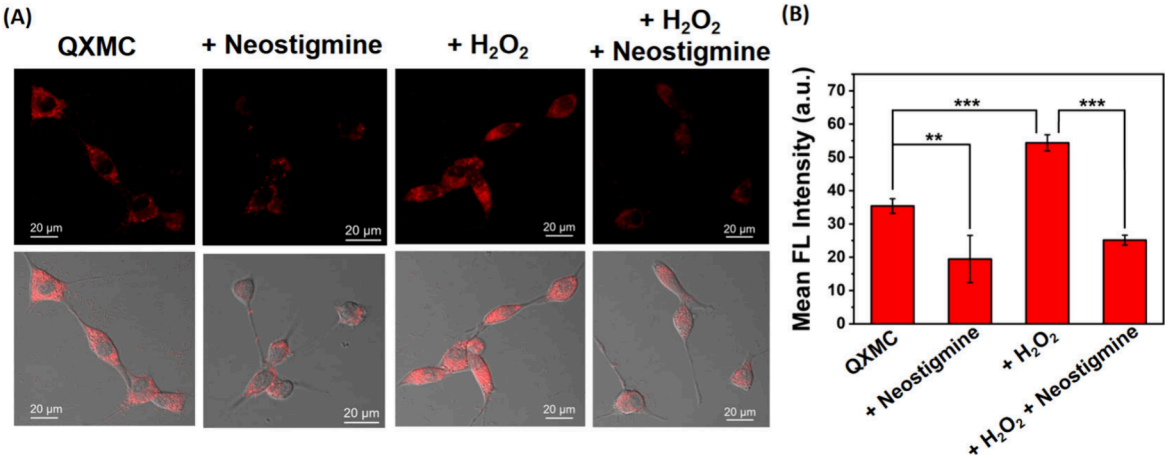

Figure 3. FL images of AChE during cell apoptosis. (A) HT22 cells were incubated with **QXMC** (5 μM, 30 min) as control; pretreated with neostigmine (100 μM, 60 min), followed by incubation with **QXMC** (5 μM, 30 min); pretreatment with H_2O_2 (100 μM, 2 h), followed by incubation with **QXMC** (5 μM, 30 min); pretreatment with neostigmine (100 μM, 60 min), followed by treatment with H_2O_2 (100 μM, 2 h), and then incubation with **QXMC** (5 μM, 30 min). (B) Mean FL intensity of images in A (±SD, n = 3, ***p < 0.001, **p < 0.01). λ_{ex} = 633 nm, λ_{em} = 640−754 nm. Scale bar: 20 μm.

stably inserted into the cavity of AChE (Figure 1A,B), which was composed of 18 active amino acid residues (Figure 1C,D). Specifically, the acetyl moiety of **QXMC** oriented toward the "esteratic" region (SER-203 and HIS-447), and the positively charged quinoline quaternary ammonium unit sited near the negative "anionic" center (Tyr-72, Tyr-337, and Asp-74), which were close to the active amino acid residues that interact with ACh. In addition, the carbonyl and xanthene groups of **QXMC** formed hydrogen-bond interactions with GLY-121, GLY-122, and TYR-124, with an average hydrogen-bond distance of 3.0 Å (Table S1), indicating a strong bonding effect between the probe and AChE, which was helpful for anchoring **QXMC** in the active pocket. Meanwhile, **QXMC** formed $\pi-\pi$ stacking interactions with TRP-286 and TYR-341 around the pocket, and hydrophobic interactions with 15 amino acids (including TYR-72, ASP-74, TRP-86, ASN-87, GLY-120, GLY-121, GLY-122, TYR-124, SER-125, SER-203, TRP-236, TRP-286, PHE-295, PHE-297, TYR-337, PHE-338, TYR-341, and HIS-447), further enhancing the stability of the **QXMC**−AChE complex. These above results demonstrated that **QXMC** and AChE had an excellent binding effect and high matching degree, and **QXMC** could be used as a potential small molecule for sensing AChE activity.

Finally, based on the above design strategy, we have successfully synthesized **QXMC** (Scheme S1), and the characterization by nuclear magnetic resonance (NMR) and high-resolution mass spectrometry (HRMS) was presented in the Supporting Information (Figures S1−S10).

Optical Response of QXMC toward AChE

The spectral response of **QXMC** toward AChE was investigated in CH_3CN/PBS (1/49, v/v, pH 7.4). As shown in Figure S11, **QXMC** exhibited an absorption at 520 nm (ε_1 = 2.57 × 10^4 L mol^{-1} cm^{-1}), while a red-shifted absorption of 570 nm (ε_1 = 2.57 × 10^4 L mol^{-1} cm^{-1}) was observed in QXOH. In the presence of AChE, the fluorescence signal of **QXMC** considerably enhanced, which matches well with that of QXOH (Figure 2A). Considering the absolute signal strength, low background level, and compatibility with fluorescence imaging laser, the long wavelength of 633 nm is chosen as the optimal excitation wavelength for AChE activity detection (Figure S12). As shown in Figure 2B, **QXMC** exhibited a faint fluorescence at 678 nm. Upon addition of AChE activity from 0 to 2.0 U/mL, a progressive increase in fluorescence intensity was observed, with a 5.4-fold enhancement response when the AChE activity reached 2.0 U/mL. This could be attributed to the hydrolysis by AChE and thereby the release of fluorescent QXOH, as proposed in Scheme 1. The FL intensity at $I_{678\,nm}$ displayed excellent linear relationship with the AChE activity over the range of 0−2.0 U/mL ($I_{678\,nm}$ = 63169.72[AChE] (U/mL) + 35038.21, R^2 = 0.9820) (Figure 2C), and the detection limit was determined as low as 8.56 mU/mL ($3\sigma/k$), suggesting an exceptional sensitivity toward AChE (Table S2). Interestingly, **QXMC** also exhibited excellent reaction with AChE in the biological solutions such as human serum (Figure S13), further demonstrating its high sensitivity in response toward AChE.

Rapid response capability of fluorescent probes is an important guarantee for real-time detection/imaging analysis. The time-dependent kinetics of **QXMC** in the presence of 2.0 U/mL AChE was further evaluated. Surprisingly, the fluorescence intensities at 678 nm reached a maximum within only 0.5 s (Figure 2D), which is the fastest response time among the reported AChE-sensitive probes (Table S2). In addition, **QXMC** alone or in the presence of AChE displayed good photostability after excitation at 633 nm (Figure S14). The diversity of active species in biological systems may impact the response of **QXMC** to AChE; thus the selectivity of probe is the cornerstone for in vivo analysis. As such, the fluorescence response of **QXMC** in the presence of somehydrolases (2 U/mL butyrylcholinesterase, 10 U/mL esterase, and 10 U/mL pepsin), ascorbic acid, glucose, amino acids (500 μM Cys, GSH, Hcy, His, Glu, Arg, Tyr, Leu, Asp), cation (500 μM K^+, Na^+, Ba^{2+}, Fe^{3+}, Fe^{2+}, Cu^{2+}, NH_4^+), anion (500 μM CO_3^{2-}, HCO_3^-, HPO_4^{2-}, $S_2O_3^{2-}$), and reactive oxygen species (ROS, including 100 μM H_2O_2, $^1O_2$, $^{\bullet}OH$, $ONOO^-$, O_2^-) was investigated and shown in Figures 2E and S15. Encouragingly, only AChE can cause remarkable fluorescence enhancement, indicating a superb selectivity of **QXMC** toward AChE. Furthermore, **QXMC** was steady in a broad pH (3.0−10.0) range and displayed distinct fluorescence enhancement after reaction with AChE at pH 7.4 (Figure 2F), indicating that

https://doi.org/10.1021/cbmi.4c00058
Chem. Biomed. Imaging 2025, 3, 332−340

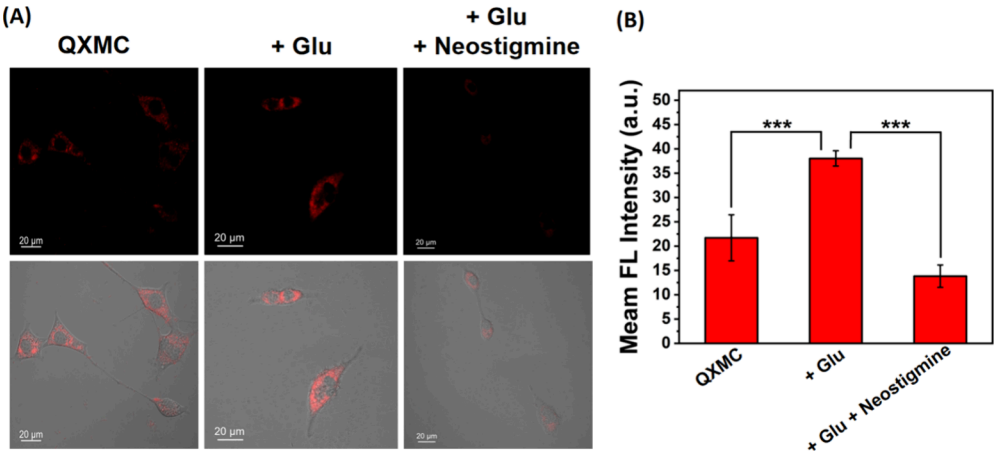

Figure 4. FL images of AChE during cell oxidative stress. (A) HT22 cells were incubated with **QXMC** (5 μM, 30 min) as control; pretreated with Glu (20 mM, 12 h), followed by incubation with **QXMC** (5 μM, 30 min); pretreatment with Glu (20 mM, 12 h), followed by treatment with neostigmine (100 μM, 60 min), and then incubation with **QXMC** (5 μM, 30 min). (B) Mean FL intensity of images in A (±SD, n = 3, ***p < 0.001). λ_{ex} = 633 nm, λ_{em} = 640−754 nm. Scale bar: 20 μm.

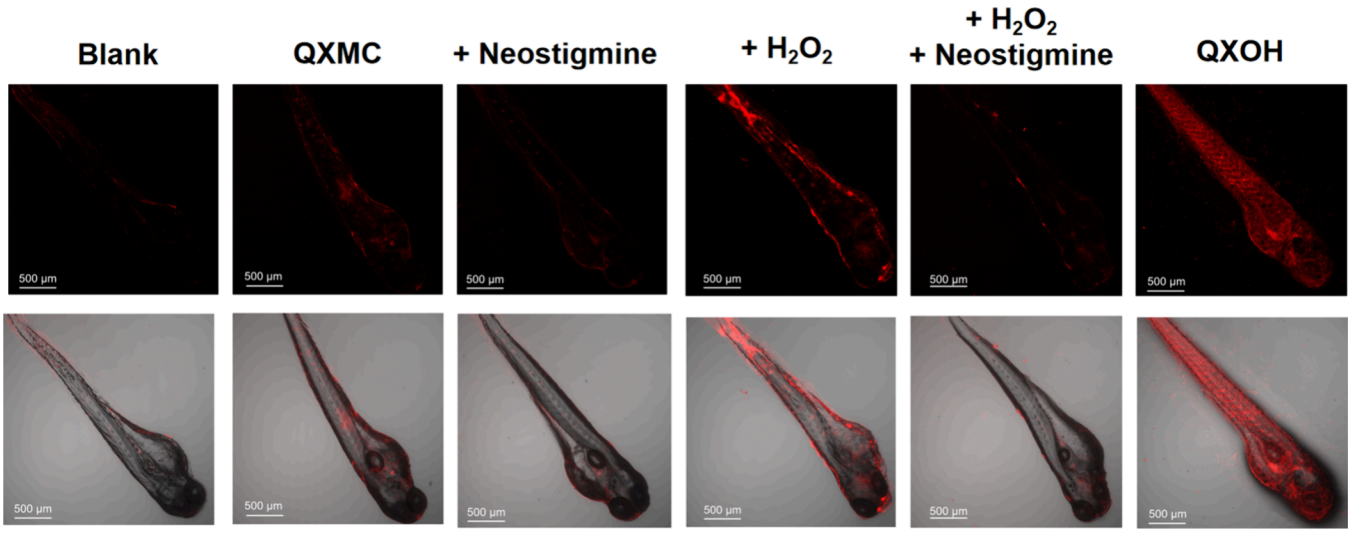

Figure 5. FL images of AChE in zebrafish. Zebrafish were treated with PBS as blank; incubated with **QXMC** (5 μM, 30 min); pretreated with neostigmine (100 μM, 60 min), followed by incubation with **QXMC** (5 μM, 30 min); pretreatment with H_2O_2 (100 μM, 60 min), followed by incubation with **QXMC** (5 μM, 30 min); pretreatment with neostigmine (100 μM, 60 min), followed by treatment with H_2O_2 (100 μM, 60 min), and then incubation with **QXMC** (5 μM, 30 min); incubation with QXOH (5 μM, 30 min). λ_{ex} = 633 nm, λ_{em} = 640−754 nm. Scale bar: 500 μm.

QXMC is very suitable for detecting AChE under physiological conditions. Collectively, the above results suggested that **QXMC** possesses high sensitivity, excellent selectivity, and ultrafast response time to AChE, making it potential for real-time imaging AChE in complex biological environments.

In order to confirm the response mechanism of **QXMC** toward AChE, the high-resolution mass spectrometry (HRMS) analysis was tested (Figures S8−S10). The free **QXMC** exhibited a mass peak at m/z = 453.2168 ([**QXMC**]$^+$, calcd: 453.2173), while in the presence of AChE, a new characteristic peak corresponding to QXOH ([QXOH]$^+$, calcd: 382.1802) was observed at m/z = 382.1800, which can be attributed to QXOH with m/z of 382.1797. The results clearly indicated that **QXMC** was transformed into QXOH after hydrolysis by AChE, fully supporting the mechanism proposed in Scheme 1.

Visualization of AChE Activity Changes in Living Cells

Delighted with the outstanding in vitro sensing ability toward AChE, **QXMC** was subsequently used for living-cell imaging. The mouse hippocampal neuron cell line (HT22) was selected as a brain-related neuronal cell model to explore the intracellular imaging potential of **QXMC**. Prior to fluorescence imaging, the toxicity of **QXMC** to HT22 cells was first evaluated using the MTT assay, as illustrated in Figure S16. An up to 88% survival rate of HT22 cells was observed when the concentration of **QXMC** was less than 10 μM, demonstrating a negligible cytotoxicity of **QXMC** on living cells under the imaging conditions (5 μM).

Emboldened by the fascinating biocompatibility, we further investigated the ability of the **QXMC** response to endogenous AChE activity changes in HT22 cells. As depicted in Figure 3A, the control cells that were only stained with **QXMC** emitted a detectable fluorescence signal within the cytoplasm, which might originate from the intrinsic AChE in HT22 cells. Interestingly, this fluorescence was obviously quenched in the cells pretreated with neostigmine (an effective AChE inhibitor currently used in clinical practice), indicating the sensitivity of **QXMC** for endogenous AChE changes. Previous studies have

https://doi.org/10.1021/cbmi.4c00058
Chem. Biomed. Imaging 2025, 3, 332−340

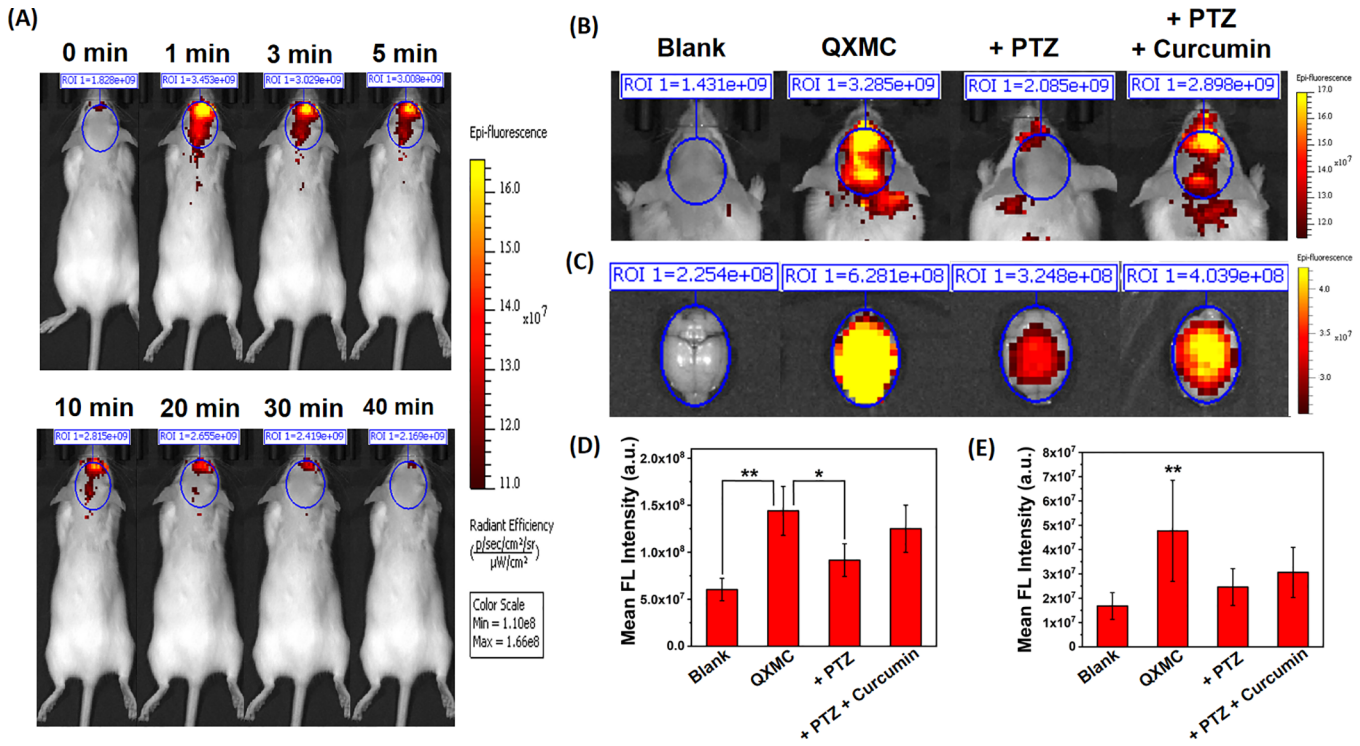

Figure 6. FL imaging of AChE in mice brain. (A) Real-time in vivo FL images of healthy mice with injection of **QXMC** (200 μM, 200 μL) through the tail vein. (B) In vivo and (C) ex vivo FL images of healthy mice and acute epileptic mice brains at 1 min postinjection of **QXMC** (200 μM, 200 μL) through the tail vein, respectively. (D,E) Mean FL intensity of images in B and C, respectively (±SD, n = 3, $^{**}p < 0.01$, $^{*}p < 0.05$). λ_{ex} = 620 nm, λ_{em} = 670 nm.

found that excessive reactive oxygen species (ROS) such as hydrogen peroxide (H_2O_2) can cause redox imbalance inside cells, inevitably triggering cell apoptosis,[39] which involves changes in AChE levels.[40] Herein, H_2O_2 was selected as a cell stimulant to construct an apoptotic cell model. As expected, the cells pretreated with H_2O_2 exhibited an enhanced fluorescence, revealing an upregulated AChE expression upon apoptosis. Similarly, neostigmine can efficiently reduce the red fluorescence, further confirming that the increased fluorescence is attributed to the overactivity of AChE during cell apoptosis. These data indicated that **QXMC** might be used as a promising candidate for studying the relationship between apoptosis and AChE.

It has been reported that high concentrations of glutamate (Glu) can induce oxidative stress in neural cells,[41] which is accompanied by AChE activity fluctuations.[19] Considering that the HT22 cell line is a favorable model for in vitro study of Glu toxicity, we attempted to observe whether AChE activity varied when HT22 cells were treated with 20 mM Glu. Consistent with the previous results, a stronger red fluorescence was captured in Glu-stimulated cells compared with the control group (Figure 4), denoting an increasing AChE level. However, the intracellular fluorescence intensity of cells pretreated with neostigmine and Glu dropped steeply, further supporting the evidence that the increase in fluorescence intensity came from high AChE activity. These observations suggested that **QXMC** has the ability to visualize endogenous AChE changes with high sensitivity at the cellular level.

Visualization of Endogenous AChE Expression in Zebrafish

Zebrafish has been widely used as a powerful vertebrate model organism to study human neurological disorders, because of its significant genetic identity with humans.[42] Particularly, AChE closely related to neurodevelopment is highly expressed in zebrafish embryos.[43] Encouraged by the satisfactory imaging results in neuronal cells, we next employed **QXMC** to visualize the endogenous AChE fluctuation in living zebrafish. As illustrated in Figure 5, zebrafish embryos of 3 days old only treated with PBS showed no fluorescence signal. After incubation with **QXMC** for 30 min, a clear red emission was detected, indicative of the activation of **QXMC** with endogenic AChE present in zebrafish. However, the zebrafish treated with neostigmine and **QXMC** together displayed negligible fluorescence, which further confirmed that the fluorescence was generated in the response of **QXMC** toward AChE in zebrafish. Next, the AChE level induced by H_2O_2 (as the apoptotic stimuli) in zebrafish was monitored. As anticipated, zebrafish pretreated with H_2O_2 exhibited a convincing fluorescence enhancement in the preoptic neuromasts, posterior neuromasts, and around the yolk sac of the zebrafish, indicating the levels of AChE in these regions are elevated during apoptosis. Similar to the cell imaging results, neostigmine could effectively eliminate this fluorescence signal by inhibiting AChE activity. It should be pointed that upon addition of QXOH, relatively uniform fluorescence was observed in the zebrafish, indicating the uniform distribution of QXOH. Interestingly, zebrafish stained with **QXMC** showed uneven fluorescence dispersion, which may be attributed to the special uneven distribution of AChE in zebrafish. Thus, the above results indicated that **QXMC** can effectively detect endogenous AChE fluctuations in zebrafish, making it a potential imaging tool for studying the function of AChE in developmental biology.

https://doi.org/10.1021/cbmi.4c00058
Chem. Biomed. Imaging 2025, 3, 332−340

Visualization of AChE in Acute Epileptic Mice Brain

Motivated by the successful application of **QXMC** in specifically imaging endogenous AChE in cells and zebrafish, we attempted to further explore the effect of **QXMC** on AChE levels in the living animal brain. It is known that the BBB is the main challenge for probes to achieve brain imaging. Fortunately, if small molecules have some appropriate physicochemical properties, then they can cross the BBB through passive diffusion. Herein, the *C* log *P* value of **QXMC** was estimated as 1.478 using ChemBioDraw 14.0,[44] indicating its suitable lipophilicity with the potential to penetrate the BBB.[45−47] The healthy mice then were injected with **QXMC** through the tail vein, and real-time in vivo fluorescence images of the mice were captured using an IVIS imaging system to observe the BBB penetration of **QXMC**. As expected, we found that **QXMC** emitted clear fluorescence in the brains (Figure 6A), which indicated that **QXMC** can effectively penetrate the BBB and react with a certain activity of AChE in the healthy brains. Notably, the NIR fluorescence signal has already reached the maximum at 1 min postinjected, and the fluorescence emission gradually weakened within 40 min. Meanwhile, there were almost no fluorescence emissions in the other parts of the mice, confirming the great potential of **QXMC** for brain imaging in vivo. In addition, to confirm the BBB penetration of the probe, the brains of healthy mice (with injection of **QXMC** through the tail vein for 1 min) and blank mice (without **QXMC** treatment) were dissected, and the olfactory bulb, hippocampus, cerebral cortex, brainstem, and cerebellar cortex were separated for ex vivo fluorescence imaging. As shown in Figure S17A, compared with the blank group, each brain tissue region of **QXMC**-treated mice shows obviously enhanced fluorescence, especially for the cerebral cortex, brainstem, and cerebellar cortex, further providing support for the excellent BBB penetration of **QXMC**.

Epilepsy as the most common neurological disorder has been regarded to be closely related to neurotransmitter imbalance during seizures. AChE can hydrolyze the cholinergic neurotransmitter ACh to maintain its level balance; monitoring AChE changes during epilepsy aids in understanding pathological mechanisms of epilepsy. Upon that, the widely used acute epilepsy mouse model was constructed by subcutaneous injection of pentylenetetrazole (PTZ, a clinical acute epileptic drug),[46] while the blank mice were injected with the same amount of physiological saline. Besides, curcumin (a neuroprotective agent with antioxidant and anti-inflammatory effects that can effectively alleviate seizures and neuronal damage) was utilized to treat the epileptic mice.[48] The in vivo fluorescence images of the mice were captured at 1 min postinjected of **QXMC**. Specifically, compared with the negligible fluorescence in blank mice without **QXMC** treatment, a strong fluorescence was observed in the healthy mice, attributed to the endogenous AChE expression in the brains (Figure 6B), whereas the fluorescence signal significantly decreased in the epileptic brain, revealing a decrease in AChE activity during PTZ-induced acute epilepsy seizures. This also indicated the potential of **QXMC** to rapidly and sensitively distinguish epilepsy from healthy mice by monitoring AChE changes through NIR fluorescence imaging. In addition, the fluorescence intensity of the brain in curcumin-treated mice was significantly enhanced compared to that of the epileptic group (Figure 6D), suggesting that relief of seizures is accompanied by an increase in AChE activity. Obviously, **QXMC** can effectively monitor this phenomenon by recording AChE changes, providing support for in vivo observation of drug intervention on epilepsy improvement. The mice then were sacrificed at 1 min postinjection of **QXMC**, and the brains were isolated for ex vivo fluorescence imaging. Consistent with the in vivo imaging results, the ex vivo brains from the epileptic group displayed a decreased fluorescence signal, and curcumin could alleviate the seizures of mice (Figure 6C and E). Taken together, the above results demonstrated that **QXMC** not only has great potential in the diagnosis of epilepsy but also in therapeutic evaluation or drug screening for epilepsy.

CONCLUSIONS

In summary, by incorporating a *N*,*N*-dimethyl carbamyl group into the quinolinium-xanthene skeleton, we presented a NIR fluorescent probe **QXMC**, for real-time and in situ imaging of AChE flux in living neuronal cells, zebrafish, and noninvasively in vivo, especially in epileptic mice brains. **QXMC** displayed excellent selectivity toward AChE and superb sensitivity (LOD = 8.56 mU/mL), which is equivalent to the lowest level among the previous probes. Surprisingly, **QXMC** showed the fastest response time (within 0.5 s) compared with currently reported probes. Combining **QXMC** and confocal fluorescence imaging, we demonstrated an overproduced AChE in living cells and zebrafish during apoptosis or the oxidative stress process. Most importantly, facilitated by the distinguished BBB penetration ability of **QXMC**, for the first time, a decrease in AChE activity in the acute epileptic mice brains and a recovery of AChE level in curcumim administrating epilepsy were disclosed, making **QXMC** an effective imaging tool for promoting the pathogenesis research and treatment of epilepsy. We also envision that **QXMC** can be extended to the early diagnosis, therapeutic evaluation, and drug screening of other AChE-related neurological diseases, which may further accelerate the development of new activatable probes that can be used in real-world biomedical applications.

ASSOCIATED CONTENT

Supporting Information

The Supporting Information is available free of charge at https://pubs.acs.org/doi/10.1021/cbmi.4c00058.

Experimental data, including synthetic routine; optical response properties; cell cytotoxicity; fluorescence images; and ^{1}H NMR, ^{13}C NMR, and HR−MS spectra (PDF)

AUTHOR INFORMATION

Corresponding Authors

Li Fan − *Institute of Environmental Science, School of Chemistry and Chemical Engineering, Shanxi University, Taiyuan 030006, People's Republic of China*; orcid.org/0009-0000-2721-0612; Email: fanli128@sxu.edu.cn

Xue Yu − *School of Chemistry and Pharmaceutical Engineering, Jilin Institute of Chemical Technology, Jilin 132022, China*; Email: dongjibinghuayuxue@163.com

Xihua Yang − *Laboratory Animal Center, Shanxi Province Cancer Hospital/Shanxi Hospital Affiliated to Cancer Hospital, Chinese Academy of Medical Sciences/Cancer Hospital Affiliated to Shanxi Medical University, Taiyuan 030013, People's Republic of China*; Email: yangxihua@126.com

Chuan Dong − *Institute of Environmental Science, School of Chemistry and Chemical Engineering, Shanxi University, Taiyuan 030006, People's Republic of China;* orcid.org/0000-0002-1827-8794; Email: dc@sxu.edu.cn

Authors

Rui Wang − *Institute of Environmental Science, School of Chemistry and Chemical Engineering, Shanxi University, Taiyuan 030006, People's Republic of China*

Qi Zan − *Institute of Environmental Science, School of Chemistry and Chemical Engineering, Shanxi University, Taiyuan 030006, People's Republic of China*

Kunyi Zhao − *Institute of Environmental Science, School of Chemistry and Chemical Engineering, Shanxi University, Taiyuan 030006, People's Republic of China*

Yuewei Zhang − *School of Chemistry and Pharmaceutical Engineering, Jilin Institute of Chemical Technology, Jilin 132022, China;* orcid.org/0000-0001-6696-0336

Yunong Huang − *School of Chemistry and Pharmaceutical Engineering, Jilin Institute of Chemical Technology, Jilin 132022, China*

Yongming Yang − *Laboratory Animal Center, Shanxi Province Cancer Hospital/Shanxi Hospital Affiliated to Cancer Hospital, Chinese Academy of Medical Sciences/Cancer Hospital Affiliated to Shanxi Medical University, Taiyuan 030013, People's Republic of China*

Wenjing Lu − *Institute of Environmental Science, School of Chemistry and Chemical Engineering, Shanxi University, Taiyuan 030006, People's Republic of China;* orcid.org/0000-0003-4702-5777

Shaomin Shuang − *Institute of Environmental Science, School of Chemistry and Chemical Engineering, Shanxi University, Taiyuan 030006, People's Republic of China;* orcid.org/0000-0003-2880-5444

Complete contact information is available at: https://pubs.acs.org/10.1021/cbmi.4c00058

Notes

The authors declare no competing financial interest.

■ ACKNOWLEDGMENTS

This work was supported by the National Natural Science Foundation of China (81901814, 22306114, 22274090, and 82473961), the Fundamental Research Program of Shanxi Province (202303021221066), the Central Guides Local Fund for Science and Technology Development (YDZJSX20231A008), the Graduate Student Education Innovation project (SXU2022Y159), the Program of Science and Technology Development Plan of Jilin Province (YDZJ202301ZYTS312, YDZJ202201ZYTS618), and Outstanding Youth Training Program of Jilin City (20230103015). We also appreciate Fei Zhang from SCI-GO (www.sci-go.com) for the molecular docking simulations.

■ REFERENCES

(1) Ding, D.; Zhou, D.; Sander, J. W.; Wang, W. Z.; Li, S. C.; Hong, Z. Epilepsy in China: major progress in the past two decades. *Lancet Neurol.* **2021**, *20*, 316−326.

(2) Falco-Walter, J. Epilepsy-Definition, Classification, Pathophysiology, and Epidemiology. *Semin. Neurol.* **2020**, *40*, 617−623.

(3) Kwan, P.; Arzimanoglou, A.; Berg, A. T.; Brodie, M. J.; Allen Hauser, W.; Mathern, G.; Moshé, S. L.; Perucca, E.; Wiebe, S.; French, J. Definition of drug resistant epilepsy: Consensus proposal by the ad hoc Task Force of the ILAE Commission on Therapeutic Strategies. *Epilepsia* **2010**, *51*, 1069.

(4) Baig, A. M.; Rana, Z.; Tariq, S.; Lalani, S.; Ahmad, H. R. Traced on the Timeline: Discovery of Acetylcholine and the Components of the Human Cholinergic System in a Primitive Unicellular Eukaryote Acanthamoeba spp. *ACS Chem. Neurosci.* **2018**, *9*, 494−504.

(5) Soreq, H.; Seidman, S. Acetylcholinesterase-new roles for an old actor. *Nat. Rev. Neurosci.* **2001**, *2* (4), 294−302.

(6) Talesa, V. N. Acetylcholinesterase in Alzheimer's disease. *Mech. Ageing Dev.* **2001**, *122*, 1961−1969.

(7) Mineur, Y. S.; Obayemi, A. M.; Wigestrand, B. G.; Fote, M.; Calarco, C. A.; Li, A. M.; Picciotto, M. R. Cholinergic signaling in the hippocampus regulates social stress resilience and anxiety-and depression-like behavior. *Proc. Natl. Acad. Sci. U. S. A.* **2013**, *110*, 3573−3578.

(8) Costa, D. A.; de Oliveira, G. A. L.; Lima, T. C.; dos Santos, P. S.; de Sousa, D. P.; de Freitas, R. M. Anticonvulsant and Antioxidant Effects of Cyano-carvone and Its Action on Acetylcholinesterase Activity in Mice Hippocampus. *Cell Mol. Neurobiol.* **2012**, *32*, 633−640.

(9) Sales, I. M. S.; Freitas, R. L. M.; Saldanha, G. B.; Souza, G. F.; Freitas, R. M. Choline acetyltransferase and acetylcholinesterase activities are reduced in rat striatum and frontal cortex after pilocarpine-induced seizures. *Neurosci. Lett.* **2010**, *469*, 81−83.

(10) Anesti, M.; Stavropoulou, N.; Atsopardi, K.; Lamari, F. N.; Panagopoulos, N. T.; Margarity, M. Effect of rutin on anxiety-like behavior and activity of acetylcholinesterase isoforms in specific brain regions of pentylenetetrazol-treated mice. *Epilepsy Behav.* **2020**, *102*, 106632.

(11) Gnatek, Y.; Zimmerman, G.; Goll, Y.; Najami, N.; Soreq, H.; Friedman, A. Acetylcholinesterase loosens the brain's cholinergic anti-inflammatory response and promotes epileptogenesis. *Front. Mol. Neurosci.* **2012**, *5*, 1−9.

(12) Zimmerman, G.; Njunting, M.; Ivens, S.; Tolner, E.; Behrens, C. J.; Gross, M.; Soreq, H.; Heinemann, U.; Friedman, A. Acetylcholineinduced seizure-like activity and modified cholinergic gene expression in chronically epileptic rats. *Eur. J. Neurosci.* **2008**, *27*, 965−975.

(13) Li, Z.; Wang, C.; Zhang, X. M.; Li, S. J.; Mao, Z. Q.; Liu, Z. H. Activatable luminescent probes for imaging brain diseases. *Nano Today.* **2021**, *39*, 101239.

(14) Han, H. H.; Tian, H.; Zang, Y.; Sedgwick, A. C.; Li, J.; Sessler, J. L.; He, X. P.; James, T. D. Small-molecule fluorescence-based probes for interrogating major organ diseases. *Chem. Soc. Rev.* **2021**, *50*, 9391−9429.

(15) Mao, Z.; Xiong, J.; Wang, P.; An, J.; Zhang, F.; Liu, Z.; Seung Kim, J. Activity-based fluorescence probes for pathophysiological peroxynitrite fluxes. *Coord. Chem. Rev.* **2022**, *454*, 214356.

(16) Geng, Y. J.; Wang, Z.; Zhou, J. Y.; Zhu, M. G.; Liu, J.; James, T. D. Recent progress in the development of fluorescent probes for imaging pathological oxidative stress. *Chem. Soc. Rev.* **2023**, *52* (11), 3873−3926.

(17) Yu, X.; Huang, Y. N.; Tao, Y. Q.; Fan, L.; Zhang, Y. W. Mitochondria-targetable small molecule fluorescent probes for the detection of cancer-associated biomarkers: A review. *Anal. Chim. Acta* **2024**, *1289*, 342060.

(18) An, J. M.; Jung, K. O.; Oh, M. S.; Kim, D. Acetylcholinesterase-responsive fluorescent probe: Recent advances from development to applications. *Dyes Pigments.* **2023**, *215*, 111267.

(19) Wang, X.; Li, P.; Ding, Q.; Wu, C. C.; Zhang, W.; Tang, B. Observation of Acetylcholinesterase in Stress-Induced Depression Phenotypes by Two-Photon Fluorescence Imaging in the Mouse Brain. *J. Am. Chem. Soc.* **2019**, *141*, 2061−2068.

(20) Wu, X.; An, J. M.; Shang, J.; Huh, E.; Qi, S.; Lee, E.; Li, H.; Kim, G.; Ma, H.; Oh, M. S.; Kim, D.; Yoon, J. A molecular approach to rationally constructing specific fluorogenic substrates for the detection of acetylcholinesterase activity in live cells, mice brains and tissues. *Chem. Sci.* **2020**, *11* (41), 11285−92.

(21) Ma, J. L.; Si, T. T.; Yan, C. X.; Li, Y. J.; Li, Q.; Lu, X. F.; Guo, Y. Near-Infrared Fluorescence Probe for Evaluating Acetylcholinesterase Activity in PC12 Cells and In Situ Tracing AChE Distribution in Zebrafish. *ACS Sens.* **2020**, *5*, 83−92.
(22) Ma, Y. Y.; Gao, W. J.; Ma, S. H.; Liu, Y. Y.; Lin, W. Y. Observation of the Elevation of Cholinesterase Activity in Brain Glioma by a Near-Infrared Emission Chemsensor. *Anal. Chem.* **2020**, *92*, 13405−13410.
(23) He, N.; Yu, L.; Xu, M. H.; Huang, Y.; Wang, X. Y.; Chen, L. X.; Yue, S. W. Near-infrared fluorescent probe for evaluating the acetylcholinesterase effect in the aging process and dietary restriction via fluorescence imaging. *J. Mater. Chem. B* **2021**, *9*, 2623−2630.
(24) Oe, M.; Miki, K.; Masuda, A.; Nogita, K.; Ohe, K. An activator-induced quencherdetachment-based turn-on probe with a cationic substrate moiety for acetylcholinesterase. *Chem. Commun.* **2022**, *58*, 1510.
(25) Fortibui, M. M.; Jang, M.; Lee, S.; Ryoo, I.-J.; Ahn, J. S.; Ko, S.-K.; Kim, J. Near-Infrared fluorescence probe for specific detection of acetylcholinesterase and imaging in live cells and zebrafish. *ACS Appl. Bio. Mater.* **2022**, *5* (5), 2232−2239.
(26) Wu, Z. H.; Hao, Z. X.; Chai, Y. F.; Li, A. P.; Wang, C.; Zhang, X. C.; Chen, H. P.; Lu, C. Y. Near-infrared-excitable acetylcholinesterase-activated fluorescent probe for sensitive and anti-interference detection of pesticides in colored food. *Biosens. Bioelectron.* **2023**, *233*, 115341.
(27) Wei, X. Z.; Zhu, T.; Ma, Y. S.; Sun, J. Y.; Zheng, G. X.; Ma, T. B.; Yang, X. F.; Song, Z. L.; Lv, Y. F.; Zhang, J.; Yan, M. Monitoring acetylcholinesterase level changes under oxidative stress through ESIPT-ICT-based near-infrared fluorescent probe. *Sensor Actuat. B-Chem.* **2023**, *380*, 133392.
(28) Xing, L.; Ma, P. Y.; Chen, F. F. A novel turn-on near-infrared fluorescent probe for highly sensitive *in vitro* and *in vivo* detection of acetylcholinesterase activity. *Spectrochim. Acta. A* **2024**, *310*, 123954.
(29) Tang, X. J.; Zhang, Y.; Wang, Q. Y.; Li, Z.; Zhang, C. X. Detection of acetylcholinesterase and butyrylcholinesterase in vitro and in vivo using a new fluorescent probe. *Chem. Commun.* **2024**, *60*, 2082.
(30) Meng, W. Q.; Pei, Z. P.; Wang, Y. R.; Sun, M. X.; Xu, Q. Q.; Cen, J. F.; Guo, K.; Xiao, K.; Li, Z. J. Two birds with one stone: The detection of nerve agents and AChE activity with an ICT-ESIPT-based fluorescence sensor. *J. Hazard. Mater.* **2021**, *410*, 124811.
(31) Xiang, C. B.; Dirak, M.; Luo, Y.; Peng, Y. L.; Cai, L. T.; Gong, P.; Zhang, P. F.; Kolemen, S. A responsive AIE-active fluorescent probe for visualization of acetylcholinesterase activity in vitro and *in vivo*. *Mater. Chem. Front.* **2022**, *6*, 1515−1521.
(32) Yao, M.; Nie, H. L.; Yao, W. X.; Yang, X. P.; Zhang, G. W. A sensitive and selective fluorescent probe for acetylcholinesterase: Synthesis, performance, mechanism and application. *Arab. J. Chem.* **2022**, *15*, 103929.
(33) Sidhu, J. S.; Rajendran, K.; Mathew, A. B.; Iqbal, T.; Saini, D. K.; Das, D. Acetylcholine Structure-Based Small Activatable Fluorogenic Probe for Specific Detection of Acetylcholinesterase. *Anal. Chem.* **2023**, *95*, 7594−7602.
(34) Abbott, N. J.; Patabendige, A. A. K.; Dolman, D. E. M.; Yusof, S. R.; Begley, D. J. Structure and function of the blood-brain barrier. *Neurobiol. Dis.* **2010**, *37*, 13−25.
(35) Li, H. D.; Kim, D.; Yao, Q. C.; Ge, H. Y.; Chung, J.; Fan, J. L.; Wang, J. Y.; Peng, X. J.; Yoon, J. Activity-based NIR fluorescent probes based on the versatile hemicyanine scaffold: design strategy, biomedical applications, and outlook. *Chem. Soc. Rev.* **2022**, *51*, 1795−1835.
(36) Jeong, H.; Wu, X. F.; Lee, J.-S.; Yoon, J. Recent advances in enzyme-activated NIR fluorescent probes for biological applications. *Trends in Anal. Chem.* **2023**, *168*, 117335.
(37) Wang, F. F.; Zhong, Y. T.; Bruns, O.; Liang, Y. Y.; Dai, H. J. In vivo NIR-II fluorescence imaging for biology and medicine. *Nat. Photonics.* **2024**, *18*, 535−547.
(38) Zhao, J.; Wang, C.; Sun, W. B.; Li, C. Tailoring Materials for Epilepsy Imaging: From Biomarkers to Imaging Probes. *Adv. Mater.* **2022**, *34*, 2203667.
(39) Zhang, Y. W.; Wang, S. H.; Zhang, N.; Wang, X. D.; Zan, Q.; Fan, L.; Yu, X.; Shuang, S. M.; Dong, C. Three birds with one stone: a single AIEgen for dual-organelle imaging, cell viability evaluation and photodynamic cancer cell ablation. *Mater. Chem. Front.* **2022**, *6*, 333−340.
(40) Zhang, X. J.; Greenberg, D. S. Acetylcholinesterase involvement in apoptosis. *Front. Mol. Neurosci.* **2012**, *5*, 40.
(41) Choi, D. W. Glutamate neurotoxicity and diseases of the nervous system. *Neuron.* **1988**, *1*, 623−634.
(42) Seth, A.; Stemple, D. L.; Barroso, I. The emerging use of zebrafish to model metabolic disease. *Dis. Models Mech.* **2013**, *6*, 1080−1088.
(43) Behra, M.; Cousin, X.; Bertrand, C.; Vonesch, J.-L.; Biellmann, D.; Chatonnet, A.; Strahle, U. Acetylcholinesterase is required for neuronal and muscular development in the zebrafish embryo. *Nat. Neurosci.* **2002**, *5*, 111−118.
(44) Fan, L.; Wang, X. D.; Zan, Q.; Yang, Y.; Li, F.; Zhang, C.; Shuang, S. M.; Dong, C. Lipid droplet-specific fluorescent probe for *in vivo* visualization of polarity in fatty liver, inflammation, and cancer models. *Anal. Chem.* **2021**, *93*, 8019−8026.
(45) Jagtiani, E.; Yeolekar, M.; Naik, S.; Patravale, V. In vitro blood brain barrier models: An overview. *J. Controlled Release* **2022**, *343*, 13−30.
(46) Yan, H. M.; Wang, Y. T.; Huo, F. J.; Yin, C. X. Fast-Specific Fluorescent Probes to Visualize Norepinephrine Signaling Pathways and Its Flux in the Epileptic Mice Brain. *J. Am. Chem. Soc.* **2023**, *145*, 3229−3237.
(47) Yang, Y.; Zhang, Y.; Ma, M.; Liu, H.; Ge, K.; Zhang, C.; Jin, M.; Liu, D.; Wang, S.; Yin, C.; Zhang, J. Synergistic Modulation by Halogens and Pyridine Crossing the Blood-Brain Barrier for In Situ Visualization of Thiol Flux in the Epileptic Brain. *Anal. Chem.* **2022**, *94*, 14443−14452.
(48) Hu, J. S.; Shao, C. W.; Wang, X. A.; Di, X. J.; Xue, X. L.; Su, Z.; Zhao, J.; Zhu, H.-L.; Liu, H. K.; Qian, Yong. Imaging Dynamic Peroxynitrite Fluxes in Epileptic Brains with a Near-Infrared Fluorescent Probe. *Adv. Sci.* **2019**, *6*, 1900341.

https://doi.org/10.1021/cbmi.4c00058
Chem. Biomed. Imaging 2025, 3, 332−340